Chemical routes to materials

Co-deposition of Ag and Co_3O_4 on black TiO_{2-x} nanotubes with enhanced photocatalytic activity under visible light irradiation

Ting Zhang[1], Tingxuan Yang[1], Saifang Huang[1,2], Yuguang Pu[1], Shanghai Wei[1], and Wei Gao[1,*]

[1] *Department of Chemical and Materials Engineering, the University of Auckland, Private Bag 92019, Auckland 1142, New Zealand*
[2] *School of Materials Science and Engineering, Jiangsu University of Science and Technology, Zhenjiang 212003, P. R. China*

ABSTRACT

Due to the development of industries, environmental problems attract much attention, and photocatalyst degradation of dye materials has been considered an effective way to solve the problems. Herein, the strategy that decorates Ag and Co_3O_4 nanoparticles on the black TiO_{2-x} nanotube arrays substrate (Ag/Co_3O_4/TiO_{2-x}@Ti) is constructed to enhance the photodegradation properties of the catalyst under visible light irradiation. The composite Ag/Co_3O_4/TiO_{2-x}@Ti demonstrates enhanced visible light absorption due to the local surface plasmon resonance (LSPR) of Ag nanoparticles as well as the formation of oxygen vacancy and Ti^{3+} in black TiO_{2-x} nanotube arrays substrate. Moreover, the Ag/Co_3O_4/TiO_{2-x}@Ti exhibit enhanced degradation performance compared to the single Ag/TiO_{2-x}@Ti system, the photocatalytic efficiency of Ag/Co_3O_4/TiO_{2-x}@Ti in degradation MB was 1.2 times higher. Furthermore, the photocatalyst performance of Ag/Co_3O_4/TiO_{2-x}@Ti in the degradation of MB is 1.5 and 5.2 times higher than that of black TiO_{2-x} nanotube arrays and white TiO_2 nanotube arrays, respectively. The improved photocatalytic activities can be attributed to the effect of the strong absorption under visible light, the effective separation of electrons and holes during the reaction, and the decreased bandgap due to the black TiO_{2-x}.

Handling Editor: Christopher Blanford.

Address correspondence to E-mail: w.gao@auckland.ac.nz

🖄 Springer

GRAPHICAL ABSTRACT
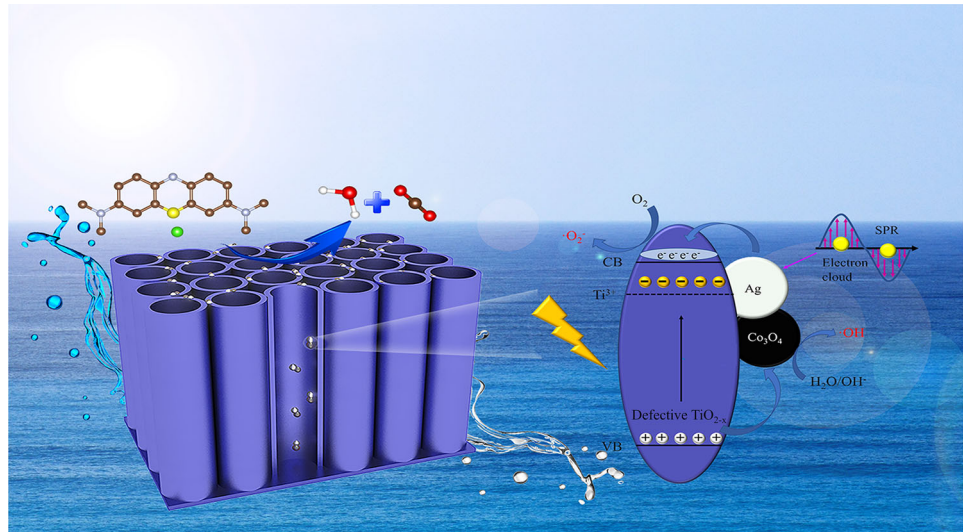
Introduction

The dyes as an industrial pollutant have caused serious environmental and health issues [1–4]. There are around 10–15% of dye left after the dyeing process and released into nature water from wasted industrial solution [5, 6]. Synthesized dye materials are usually hard to be degraded in a natural environment due to their stable chemical state [7–10]. Therefore, it is urgent to find better methods to eliminate synthesized dye materials from wasted water.

Semiconductor-based catalysts have widely been used as photocatalyst materials to degrade organic dyes under UV or visible light energy due to the non-toxic and use friendly [11–13]. TiO_2 is one of the most popular photocatalysts because of its high stability and low cost [9, 14]. However, TiO_2 photocatalysts suffer from the fast recombination of light excited electrons and holes [15–17]. In addition, the visible light absorption and conductivity of the noble metal-based TiO_2 photocatalysts are still rather low.

Several methods, including structure design [18], doping with metal and nonmetal atoms [19, 20], surface photosensitization [21], and a combination of other semiconductors [22–25] have been attempted to improve the photocatalytic performance of TiO_2. Heterojunctions between TiO_2 and other semiconductors have been recognized as an effective way to separate electrons and holes, which can increase the photocatalytic performance of the catalyst. Co_3O_4 is a kind of *p*-type transition metal oxide semiconductor material with a low bandgap (1.2–2.1 eV), which can be excited by visible light during photocatalytic reactions [26–28]. In addition, the excellent chemical stability and sensitive response of light irradiation make Co_3O_4 much attractive to researchers [29]. The combination of Co_3O_4 and TiO_2 also produces a Z scheme heterojunction, which prevents the electron–hole recombination and boosts the photoinduced carriers transfer [30]. Furthermore, the effect of LSPR by noble metals such as Ag and Au can play the role of electron trap center to separate the electrons and holes [31]. Due to the strong absorption of visible light of noble metal, the metal particles combine with TiO_2 to achieve high photocatalyst activity.

The black TiO_{2-x} has been synthesized by the hydrogen annealing process [32]. The formation of oxygen vacancy and Ti^{3+} in the black TiO_{2-x} significantly decreases the bandgap and increases the visible light absorption. Due to these advantages, black

TiO_{2-x} can be used to substitute for pure TiO_2 as a photocatalyst. Reports indicated that black-TiO_2/$CoTiO_3$ nanocomposite exhibits a good degradation efficiency to remove 99% of rhodamine B (RhB), methylene blue, and methyl orange (MO) [33]. A nano-photocatalyst consisting of reduced graphene oxide (RGO), black TiO_{2-x} nanosheet, and 2-D ZIF-8 sheet (2D-ZIF-8) showed high adsorption, rapid charge separation, and high efficiency of pollutions' degradation due to the formation of oxygen vacancy and double heterogeneous interface [30].

In this work, a novel nanocomposite photocatalyst $Ag/Co_3O_4/TiO_{2-x}@Ti$ was prepared through two-step anodization, electrochemical doping, and impregnating–deposition–decomposition process. Notably, the combination of Ag nanoparticles and Co_3O_4 nanoparticles with black TiO_{2-x} nanotube arrays can accept the electrons from Ag nanoparticles and transfer holes to Co_3O_4 nanoparticles, thus effectively separating electrons and holes. At the same time, the reduced bandgap of black TiO_{2-x} and LSPR effect of Ag nanoparticles can increase the light absorption from the VU range to the visible range. $Ag/Co_3O_4@TiO_{2-x}$ nanocomposite, therefore, shows much-improved photocatalyst performance with 87% degradation of MB solution in 300 min, which is 5.2 times higher than that of pure TiO_2 nanotube arrays.

Experimental

Preparation of TiO_2 nanotube arrays substrate

The highly organized TiO_2 nanotube arrays were prepared by a two-step electrochemical anodization on Ti foil (99.96%, $40 \times 25 \times 0.2$ mm^3). The Ti foil was washed with milli-Q water, acetone, and ethanol, separately. In the first anodization process, metallic Ti foil was used as the anode, and Ti mesh was applied as the cathode. Both anode and cathode were put in 250 ml electrolyte, which contains 0.25 wt% NH_4F and 2% milli-Q water in the ethylene glycol solution. The first anodization was carried out under 60 V for 24 h. After that, the formed thin TiO_2 nanotube film was removed by ultrasonication in ethanol. The second anodization was applied under 60 V for 3 h, and the TiO_2 nanotube arrays were washed in ethanol and milli-Q water. After cleaning, the

prepared sample was soaked in ethanol for 48 h to release the internal stress.

Preparation of Ag doped TiO_2 nanotube arrays substrate

Ag nanoparticles (NPs) were deposited onto TiO_2 nanotubes via electrochemical deposition. 0.1 g $AgNO_3$ was dissolved in 100 mL DI water labeled as solution A, prepared TiO_2 nanotube arrays substrate played as cathode, and Ti mesh was used as the anode, and both cathode and anode substrate were soaked in solution A. The electrochemical deposition was performed for 1 min under the voltages of 5, 10, 30, and 60 V. After electrochemical deposition, the sample was washed with milli-Q water and dried in an oven for 24 h under 60 °C. Then the dried sample was put in a tube furnace annealing in an atmosphere containing 5% H_2/95% N_2 at 550 °C for 2 h. The prepared sample was labeled as $Ag/TiO_{2-x}@Ti$.

Preparation of Ag, Co_3O_4, co-doped TiO_{2-x} nanotube arrays substrate

The deposition of Co_3O_4 nanoparticles was carried out by the impregnating–deposition–decomposition method. 8.7 g $Co(NO_3)_2$ was dissolved in 100 mL milli-Q water which was labeled as solution B. 0.12 g NaOH was dissolved in 100 mL milli-Q water which was labeled as solution C. The precursor $Co(OH)_2$ NPs were deposited on the annealed $Ag/TiO_{2-x}@Ti$ by immersing the $Ag/TiO_{2-x}@Ti$ substrate for 20 min in solution B and C separately ($Co(OH)_2/Ag/TiO_{2-x}@Ti$). After repeating the immersion procedure 3 times, $Co(OH)_2/Ag/TiO_{2-x}@Ti$ samples were dried and annealed in Ar at 220 °C for 6 h until $Co(OH)_2$ completely decomposed into Co_3O_4 NPs.

Photocatalytic property measurement

The photocatalytic activity of $Ag/Co_3O_4/TiO_{2-x}@Ti$ nanotube arrays was tested via the adsorption and decomposition of methylene blue (MB) under visible light. The catalyst films were immersed into a 50 mL MB solution (5 ppm MB), followed by stirring in the dark for 1 h to get equilibrium of adsorption/desorption of solution. A F300-W xenon lamp (BBZM-I, 380–800 nm) was applied to the solution for 4 h. The absorption spectra of the MB solution were

tested by a UV–VIS spectrophotometer with a wavelength ranging from 200 to 800 nm.

Materials characterization

The phase structure of $TiO_{2-x}@Ti$, $Ag/TiO_{2-x}@Ti$, and $Ag/Co_3O_4/TiO_{2-x}@Ti$ was analyzed by X-ray powder diffraction (XRD, Bruker D2-Phaser) with Cu Ka1 radiation (λ = 1.5406 Å) over 2θ ranging 20°-80°. The morphology and lattice structure of $Ag/Co_3O_4@TiO_{2-x}$ were characterized by high-resolution transmission electron microscopy (HRTEM, FEI Tecnai G2 F20, 200 kV). The light absorption of thin films was determined with a UV–Visible Spectrometer (Shinadzu UV-2550). The chemical state of $Ag/Co_3O_4/TiO_{2-x}@Ti$ was examined by X-ray photoelectron spectroscopy (XPS, PHI Quantera-II SXM).

Replicate syntheses

$Ag/Co_3O_4/TiO_{2-x}@Ti$ was synthesized 3 times through the same methods (repeat 1, repeat 2, and repeat 3), and the photodegradation properties of three repeat syntheses samples have been tested as the methods mentioned above.

Results and discussion

Morphology and phase structure

The preparation of $Ag/Co_3O_4/TiO_{2-x}@Ti$ is illustrated in Scheme 1. Figure 1a, b shows the powder XRD pattern of as-synthesized $Ag/Co_3O_4/TiO_{2-x}@Ti$, $Ag/TiO_{2-x}@Ti$, and $TiO_{2-x}@Ti$. For the black TiO_{2-x} nanotube arrays, all peaks are well indexed to the anatase (PDF#21–1272), rutile (PDF#89–0555), and Ti

(PDF#44–1294) phases. Compared to the black TiO_{2-x} nanotube arrays, XRD pattern of $Ag/TiO_{2-x}@Ti$ does not show any extra diffraction peaks, suggesting that only a small amount of Ag nanoparticles is loaded on the surface of the black TiO_{2-x} substrate, and the size of Ag nanoparticles is small [34, 35]. Higher doping voltages 10 V, 30 V, and 60 V were applied for Ag deposition. With increasing electrodeposition voltage, Ag peaks start to appear, as shown in Figure S1. This confirms the successful deposition of Ag NPs on the substrate.

The impregnating–deposition–decomposition and annealing methods were conducted to deposit Co_3O_4 nanoparticles on the black TiO_{2-x} nanotube arrays. Figure 1b shows the close-up XRD patterns. There are four major diffraction peaks at 31.2°, 38.8°, 59.3°, and 65.2°, corresponding to (220), (311), (511), and (440) crystal planes of Co_3O_4 (PDF#73–1701), suggesting the formation of Co_3O_4 on the black TiO_{2-x} substrate.

The morphology of as prepared black TiO_{2-x} nanotube arrays is shown in Fig. 2a. It can be seen that the nanotubes are highly ordered, and after 5 V Ag electro-doping, a small number of nanoparticles are anchored on the surface of black TiO_{2-x} surface (Fig. 2b). With increasing doping voltage from 5 to 60 V, the number of particles increases, and the size of particles increases from less than 20 nm to around 100 nm, indicating the doped particles aggregated with the increasing doping voltage (Figure S2), corresponding with the XRD results. Figure 2c shows the decoration of Co_3O_4 nanoparticles on the surface of black TiO_{2-x} nanotube arrays, exhibiting nanosheets structure. After impregnating–deposition–decomposition Co_3O_4 on the Ag particles which decorated on black TiO_{2-x} nanotube substrate, small nanoparticles change to larger nanotube structure,

Scheme 1 Preparation process of $Ag/Co_3O_4/TiO_{2-x}@Ti$.
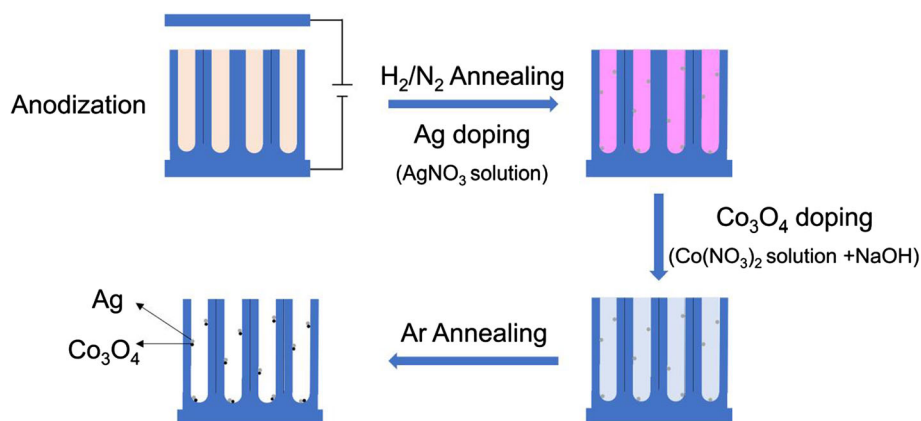
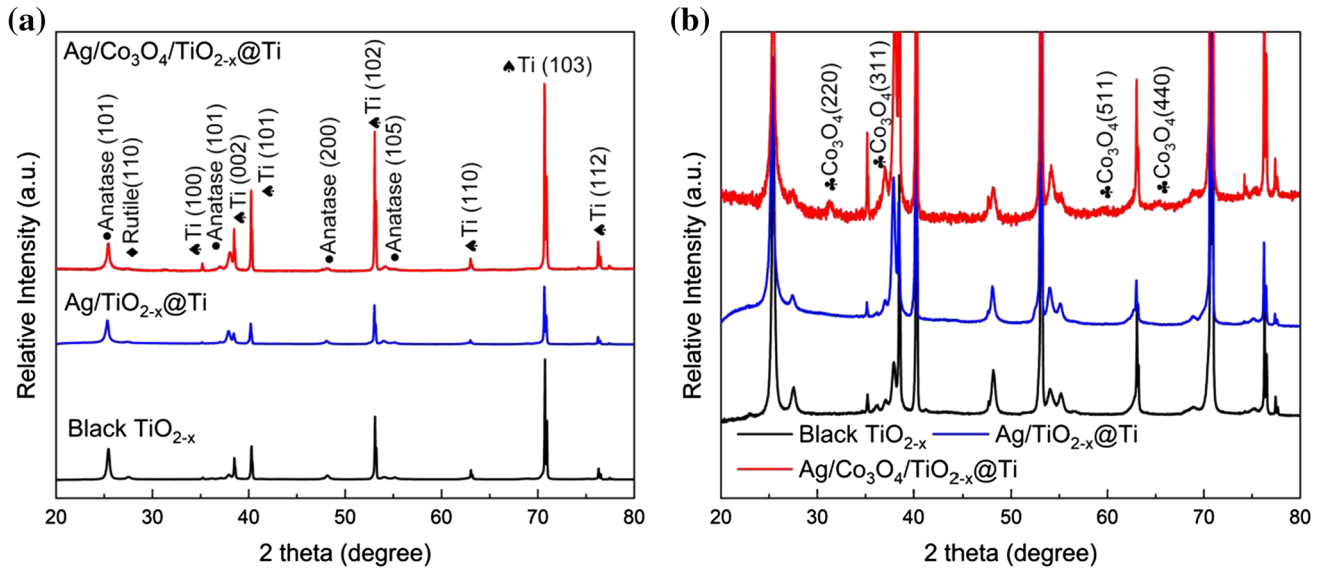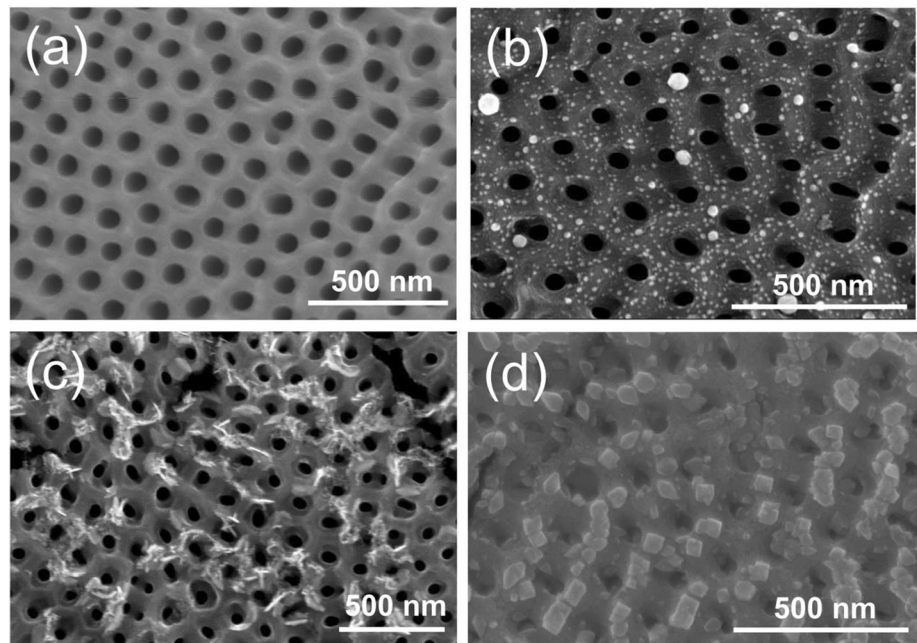**Figure 1** **a** XRD patterns and **b** close-up XRD patterns of black TiO_{2-x} nanotube arrays, $Ag/TiO_{2-x}@Ti$ and $Ag/Co_3O_4/TiO_{2-x}@Ti$.

Figure 2 SEM top view: **a** black TiO_{2-x} nanotube arrays of black TiO_{2-x}, **b** $Ag/TiO_{2-x}@Ti$, and **c** $Co_3O_4/TiO_{2-x}@Ti$, **d** $Ag/Co_3O_4/TiO_{2-x}@Ti$.

indicating the nucleation of Co_3O_4 beside the formed Ag nanoparticles (Fig. 2d).

Bright field (BF) TEM images in Figs. 3a, b, c exhibit the nanostructure of black TiO_{2-x} nanotube arrays and $Ag/Co_3O_4/TiO_{2-x}@Ti$, respectively. HR-TEM lattice images in Figs. 3d–e were acquired to further analyze the structure of the anchored nanoparticles. The lattice fringes of 0.35 nm correspond to the crystal plane of anatase TiO_2 (101). The interlayer spacing about 0.204 nm and 0.243 nm indicates the formation of Ag (200) and Co_3O_4 (311), respectively. The HR-TEM

images suggest that the Ag and Co_3O_4 nanoparticles both anchored on the black TiO_{2-x} successfully. The SAED pattern (Fig. 3f) presents the polycrystalline structure of $Ag/Co_3O_4/TiO_{2-x}@Ti$, and the ring diffraction pattern matches well with TiO_2 and Co_3O_4 phases, which agrees with the XRD results.

Figure 4 shows the XPS spectra of $Ag/Co_3O_4/TiO_{2-x}@Ti$. Figure 4a shows the high-resolution XPS spectra of Co 2p from $Ag/Co_3O_4/TiO_{2-x}@Ti$ sample, indicating Co $2p_{1/2}$ and Co $2p_{3/2}$ peaks at 796.7 eV and 783.6 eV, separately. The Co 2p spectra can be fitted into six
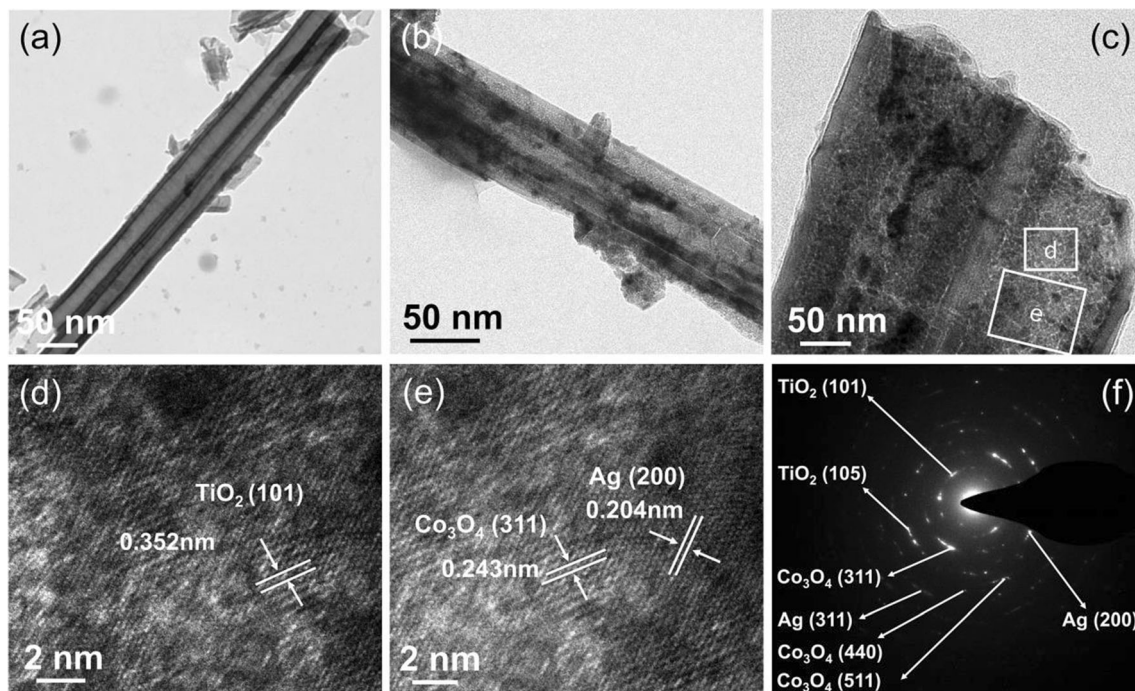
Figure 3 TEM images of **a** black TiO_{2-x}, **b** and **c** $Ag/Co_3O_4/TiO_{2-x}@Ti$, **d** and **e** high-resolution TEM image of $Ag/Co_3O_4/TiO_{2-x}@Ti$, and **f** SAED pattern of $Ag/Co_3O_4/TiO_{2-x}@Ti$.

peaks, including satellite peaks located at 786.8 and 803.0 eV, and two pairs of peaks from Co^{3+} and Co^{2+}. The energy peaks located at 780.3 eV and 794.0 eV stem from the Co^{3+} in Co $2p_{3/2}$ and Co $2p_{1/2}$, while the energy lower and higher peaks at 782.9 eV and 797.0 eV could be ascribed to Co^{2+} [36]. The existence of Co^{2+} and Co^{3+} indicates the formation of Co_3O_4 in $Ag/Co_3O_4/TiO_{2-x}@Ti$ and agrees well with the XRD results.

Figure 4b shows Ag peaks centered at 368.1 and 374.1 eV corresponding to Ag $3d_{2/3}$ and Ag $3d_{5/2}$ [37]. The separation of two peaks is 6 eV indicating the metallic nature of silver. The peaks located at 458.9 and 464.6 eV represent the $2p_{3/2}$ and $2p_{1/2}$ electronic states of normal Ti–O species, indicating the existence of Ti^{4+}. The peaks at 457.8 and 463.6 eV represent Ti–OH species, evidence of Ti^{3+} in $Ag/Co_3O_4/TiO_{2-x}@Ti$ (Fig. 4c). In the O 1 s XPS spectra (Fig. 4d), three peaks centered at 530.0, 530.6, and 532.2 eV represent the Ti–O bond in TiO_2, –OH absorption on the surface, and oxygen vacancy (Ov) neighboring Ti^{3+}, respectively [38–40].

Photocatalytic properties

UV–Vis absorbance spectra of $Ag/Co_3O_4/TiO_{2-x}@Ti$ nanotubes are shown in Fig. 5. After annealed in H_2,

black TiO_{2-x} exhibits a high absorbance ability of light, which almost covers the entire visible light region of 400–800 nm. The high visible light absorption is due to the formation of oxygen vacancy and Ti^{3+} species in black TiO_{2-x} [41–43]. Absorptions of $Ag/Co_3O_4/TiO_{2-x}@Ti$ are high in the visible light region but drop slightly after 500 nm, which may be due to the light reflection of Ag and Co_3O_4 nanoparticles on black TiO_{2-x} surface. The broad absorption peak centered around 500 nm can be attributed to the LSPR effect of Ag nanoparticles anchored on black TiO_{2-x} substrate. Compared with the sharp Ag absorption peak, the formation of a broad absorption peak is caused by the inhomogeneous particle size distribution.

The light absorption abilities of black TiO_{2-x}, $Ag/TiO_{2-x}@Ti$, and $Ag/Co_3O_4/TiO_{2-x}@Ti$ are much improved compared with the white TiO_2 substrate, indicating the high efficiency of light utilization, which could improve the photocatalyst performance of catalysts. The band gaps of these three composites are calculated by Kubelka−Munk Function (Fig. 5b). After introducing Ag and Co_3O_4, the bandgap of $Ag/Co_3O_4/TiO_{2-x}@Ti$ decreased from 3.08 to 2.57 eV, indicating that the co-deposition of Ag and Co_3O_4
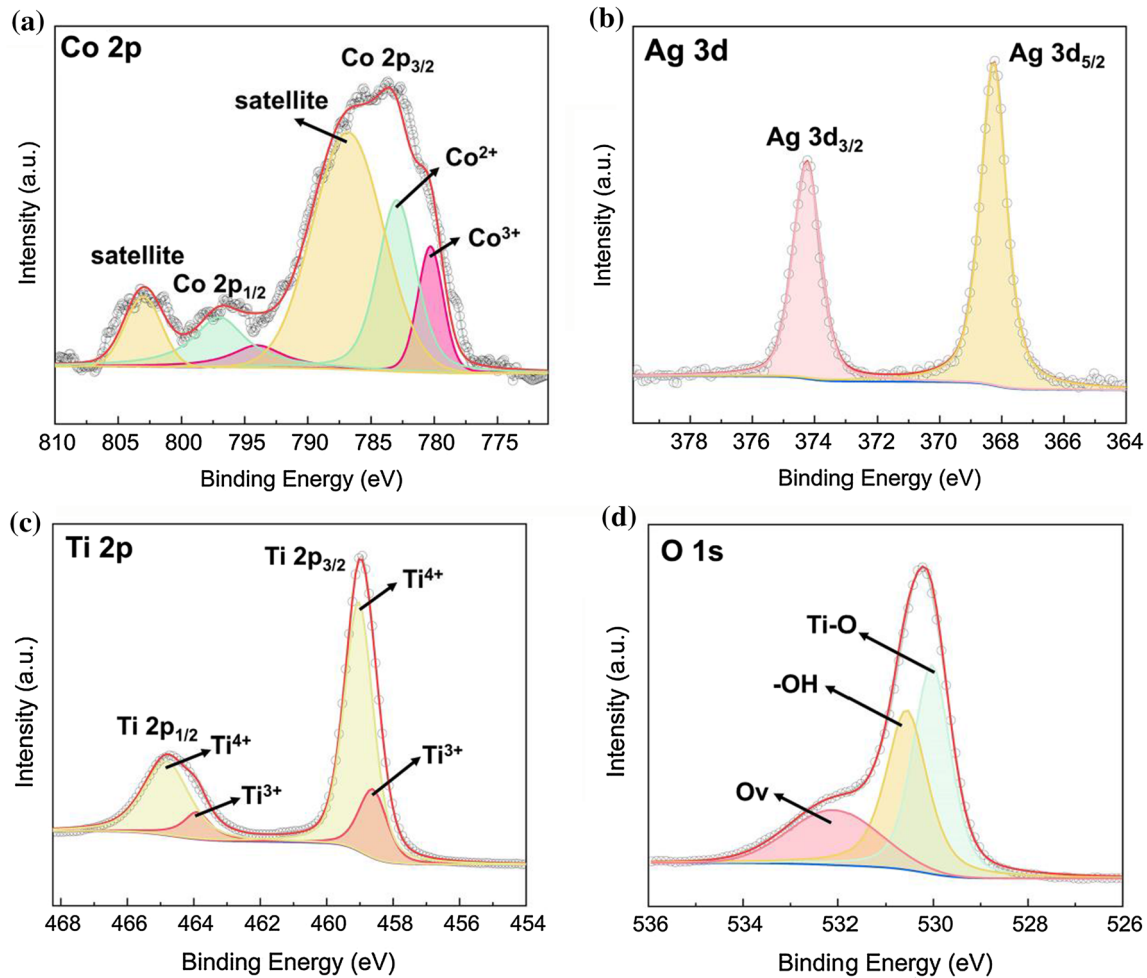
Figure 4 **a** XPS spectrum of Ag/Co$_3$O$_4$/TiO$_{2-x}$@Ti, with the corresponding high-resolution XPS spectra of **b** Co 2p, **c** Ag 3d, **d** Ti 2p and **e** O 1 s.

improves the optical properties of the TiO$_{2-x}$@Ti substrate.

Furthermore, the PL spectra for the black TiO$_{2-x}$, Ag/TiO$_{2-x}$, and Ag/Co$_3$O$_4$/TiO$_{2-x}$@Ti were plotted as revealed (Fig. 5c). The Ag doped black TiO$_{2-x}$ exhibits high charge transfer properties which result in low PL intensity compared with that of black TiO$_{2-x}$. The Ag/Co$_3$O$_4$/TiO$_{2-x}$@Ti presents the lowest PL intensity compared to the black TiO$_{2-x}$, Ag/TiO$_{2-x}$, which indicates the highest charge separation and migration properties of Ag/Co$_3$O$_4$/TiO$_{2-x}$@Ti [44]. The EIS Nyquist arc radius of Ag/Co$_3$O$_4$/TiO$_{2-x}$@Ti is smaller than that of black TiO$_{2-x}$ and Ag/TiO$_{2-x}$ (Fig. 5d), the smallest radius indicates the higher charge separation efficiency of Ag/Co$_3$O$_4$/TiO$_{2-x}$@Ti [45]. The above results further demonstrate the remarkable charge separation and migration of prepared Ag/Co$_3$O$_4$/TiO$_{2-x}$@Ti.

Photocatalytic degradation of MB of Ag/Co$_3$O$_4$/TiO$_{2-x}$@Ti nanocomposites

The photocatalytic activity of the Ag/Co$_3$O$_4$/TiO$_{2-x}$@Ti nanocomposites was tested by the degradation of methylene blue (MB) in a water solution under simulated visible light irritation. For comparison purposes, photocatalytic measurements were taken on white TiO$_2$, black TiO$_{2-x}$, and Ag/TiO$_{2-x}$@Ti samples under the same testing condition. As shown in Fig. 6a, after 60 min dark adsorption and 240 min visible irradiation, white TiO$_2$ substrate presented a low photocatalyst property at 17% compared to the black TiO$_{2-x}$ nanotubes at 58%. Deposition of Ag nanoparticles on the black TiO$_{2-x}$ substrate increases the photocatalytic property to 74%, and Ag/Co$_3$O$_4$/TiO$_{2-x}$@Ti exhibits the highest photocatalyst performance with 87% MB degraded in the solution after
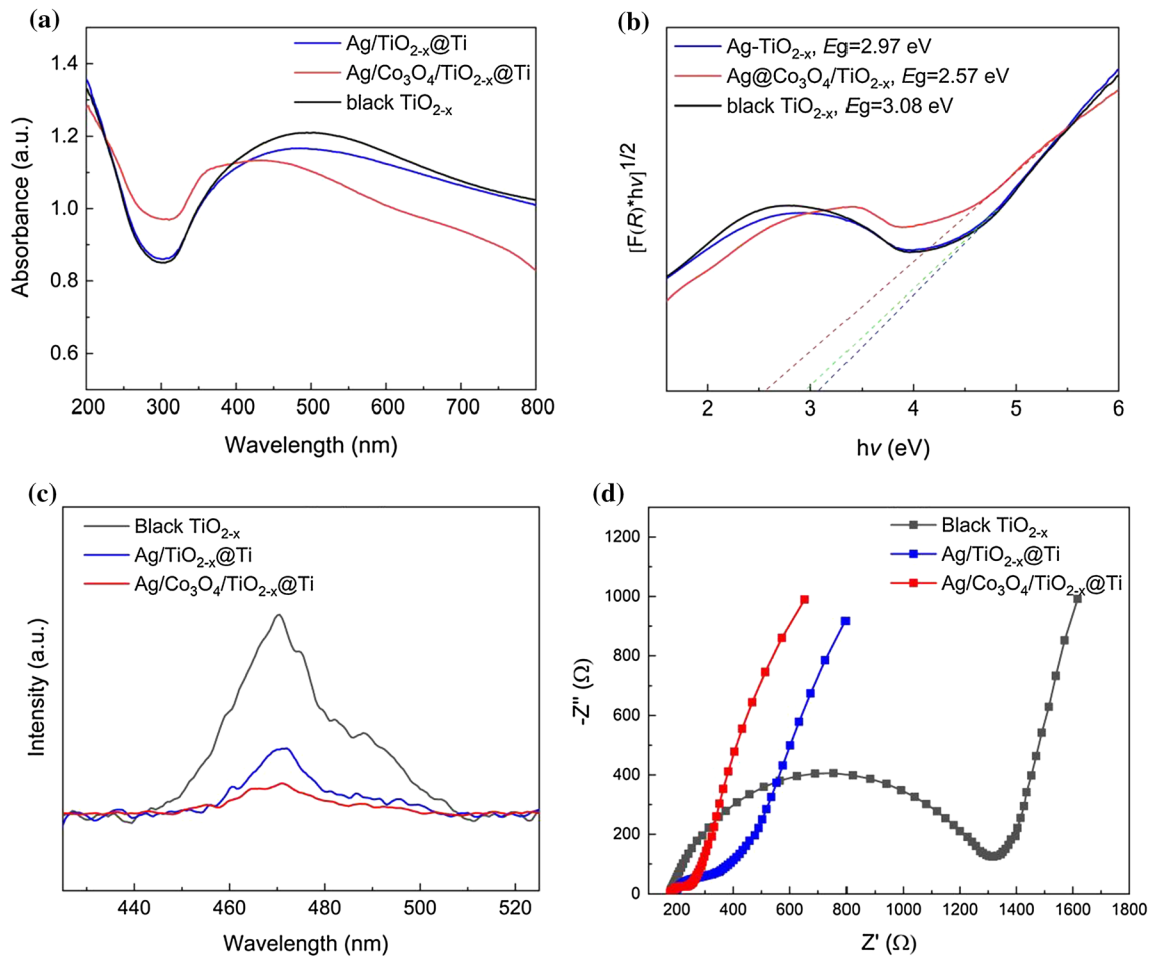
Figure 5 **a** UV–Vis absorbance spectra of black TiO_{2-x}, Ag/TiO_{2-x} and $Ag/Co_3O_4/TiO_{2-x}@Ti$, and **b** plots $(F(R)*hv)^{1/2}$ versus hv for band gap energies of black TiO_{2-x}, $Ag/TiO_{2-x}@Ti$ and $Ag/Co_3O_4/$ $TiO_{2-x}@Ti$. **c** PL spectra of black TiO_{2-x}, Ag/TiO_{2-x} and $Ag/$ $Co_3O_4/TiO_{2-x}@Ti$; **d** EIS spectra of black TiO_{2-x}, Ag/TiO_{2-x} and $Ag/Co_3O_4/TiO_{2-x}@Ti$.
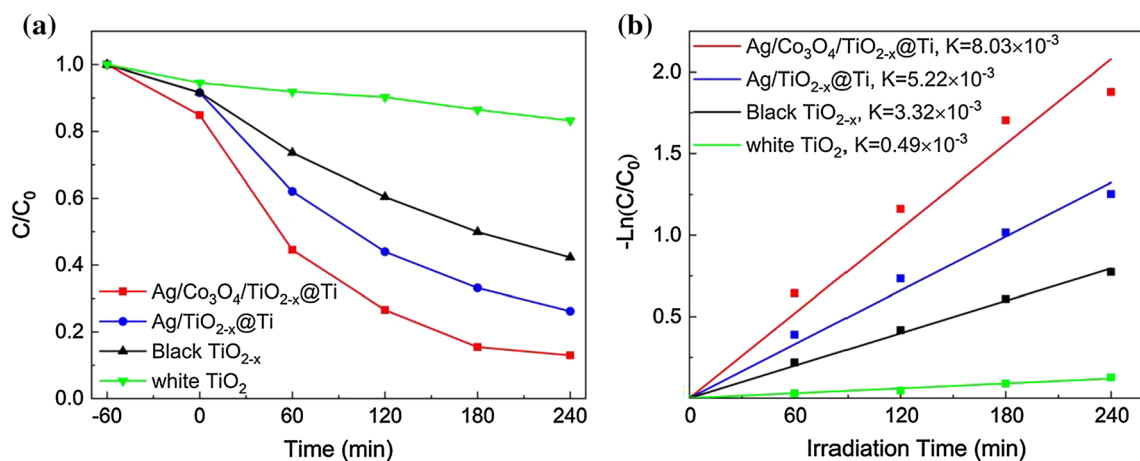

Figure 6 **a** Photocatalytic degradation of MB using a different catalyst, and **b** Langmuir–Hinshelwood model fittings of MB degradation kinetics.

dark adsorption and visible light irradiation. It is obvious that Ag and Co_3O_4 doping on black TiO_{2-x} nanotube arrays has a great effect on improving the catalytic performance. However, the photodegradation properties of the catalyst decrease with the increment of the Ag size (Figure S3). It can be explained that the superfluous Ag shielded the surface of black TiO_{2-x} substrate and reduced the number of photons reaching the inner of the nanotube. Also, more Ag content could be detrimental to photonic efficiency [46–49]. To further prove the photocatalytic properties of $Ag/Co_3O_4/TiO_{2-x}@Ti$, the catalyst has been replicated synthesized 3 times, and the repeated samples exhibit almost the same photocatalytic dye degradation performance as shown in figure S4, Figure S5.

Figure 6b shows the Langmuir–Hinshelwood kinetic fitting results, which fit well with experimental data. The regression coefficients (R^2) are higher than 0.95 with 0.957 for $Ag/Co_3O_4/TiO_{2-x}@Ti$, 0.980 for $Ag/TiO_{2-x}@Ti$, 0.985 for black TiO_{2-x}, and 0.952 for white TiO_2. At the same reaction temperature, the degradation performance of $Ag/Co_3O_4/TiO_{2-x}@Ti$ is 16 times higher than bare TiO_2. The degradation abilities and Langmuir–Hinshelwood kinetic models of different Ag doped samples are shown in Fig. S3. With increasing Ag nanoparticle size, the degradation performance decreases probably due to the larger Ag nanoparticles can act as the electrons–holes recombination sites [50], thus decreasing the amount of electrons and holes and prohibiting the photocatalyst ability during the reaction.

The structural stability and reusability of $Ag/Co_3O_4/TiO_{2-x}@Ti$ have been analyzed by the recycling, XRD, and XPS experiments. The $Ag/Co_3O_4/TiO_{2-x}@Ti$ present the unchanged photocatalyst properties after three cycles (Figure S6). The XRD spectrum of $Ag/Co_3O_4/TiO_{2-x}@Ti$ exhibits the same peaks compared with the sample before reaction, proving the crystal structure stability of $Ag/Co_3O_4/TiO_{2-x}@Ti$ (Figure S7). The XPS spectrum has been tested to verify the phase composition and elements valence of $Ag/Co_3O_4/TiO_{2-x}@Ti$ after photodegradation. After the reaction, XPS peaks of Co, Ag, Ti, and O present no obvious change, which indicates the structural stability of $Ag/Co_3O_4/TiO_{2-x}@Ti$ (Figure S8).

The mechanism of enhanced photocatalytic performance of $Ag/Co_3O_4/TiO_{2-x}@Ti$ is proposed in Fig. 7. The introduction of Ti^{3+} and oxygen vacancy into black TiO_{2-x} can generate a new energy level under the conduction band of material, thus narrowing the bandgap of black TiO_{2-x} and extending the light absorption region from UV light to visible light [51]. In this study, the formation of heterojunctions among Ag, Co_3O_4, and black TiO_{2-x} is a factor that improves the photocatalytic efficiency of black TiO_{2-x}, because the heterojunctions can act as bridges to transfer electrons and prevent the recombination of electrons and holes. Once the heterojunctions are formed, Ag particles on the surface can generate a large amount of "hot electrons" under visible-light irradiation by the unique LSPR [52]. In addition, the LSPR that comes from Ag nanoparticles is further enhanced by black TiO_{2-x} nanotubes as Ag particles doped in the black TiO_{2-x} nanotubes can absorb more scattered light [53] [54]. In this way, schottky barrier forms at the interface between Ag and black TiO_{2-x}, and hot electrons on Ag surface can migrate to the surface of black TiO_{2-x} and react with dye [55].

Co_3O_4 is a typical hole collector for oxidizing dye molecules, and the p–n junction can form at the interface between Co_3O_4 and black TiO_{2-x}, facilitating the transfer of holes from black TiO_{2-x} to Co_3O_4 and oxidizing the organic dye on the surface of Co_3O_4 [56]. Similarly, heterojunctions can be built up between Ag and Co_3O_4, providing electrons on the conduction band of Co_3O_4, which is then transferred to Ag nanoparticles and eventually to the black TiO_{2-x}. In the context of this p–n junction, organic compounds can be oxidized on Co_3O_4 surface since $Ag/Co_3O_4/TiO_{2-x}@Ti$ can use the visible light more efficiently. More electrons have been generated, and their recombination with holes is slowed down, resulting in higher photocatalytic efficiency.

Conclusions

In summary, Ag and Co_3O_4 nanoparticles were doped on black TiO_{2-x} nanotube arrays through electrochemical deposition and impregnating–deposition–decomposition methods. The presence of Ag nanoparticles, oxygen vacancy, and Ti^{3+} played an important role in the absorption of visible light during the reaction. What's more, the formation of $Ag/Co_3O_4/TiO_{2-x}@Ti$ effectively decreases the electrons and holes recombination during the reaction. The improved visible absorption and charge separation

Figure 7 Schematic of photocatalytic mechanism of $Ag/Co_3O_4/TiO_{2-x}@Ti$.
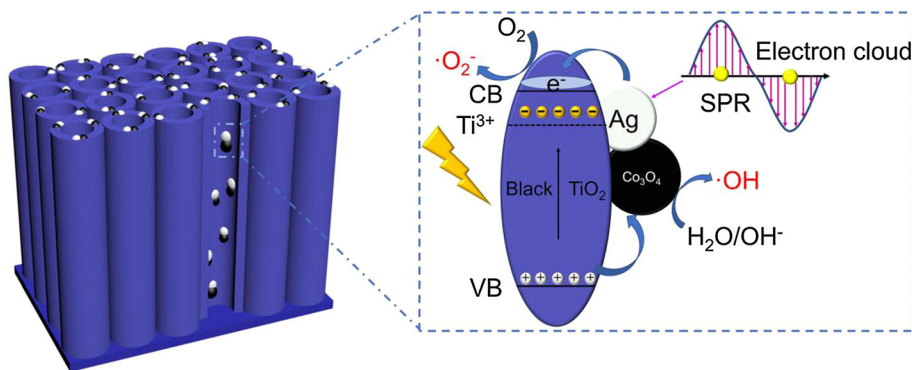
improve the photocatalyst activity for the degradation of MB under visible light. $Ag/Co_3O_4/TiO_{2-x}@Ti$ presents excellent photocatalytic efficiency, which is 5.1 times higher than that of black TiO_{2-x} under solar light irradiation. This work proposes a novel method for designing new black TiO_{2-x} based catalysts with low electron–hole recombination rate and superior photocatalytic performance.

Declarations

Conflict of interest The authors declare that they have no conflict of interest.

Supplementary Information: The online version contains supplementary material available at http s://doi.org/10.1007/s10853-021-06786-1.

References

[1] Sui X, Li X, Ni T, Lin F, Li G (2020) Carbonaceous–TiO₂ materials: unique morphologies for photocatalytic applications. J Mater Sci 55:2725

[2] Oppong SO-B, Opoku F, Anku WW, Govender PP (2021) Insights into the complementary behaviour of Gd doping in GO/Gd/ZnO composites as an efficient candidate towards photocatalytic degradation of indigo carmine dye. J Mater Sci 56:8511

[3] Anwer H, Mahmood A, Lee J, Kim K-H, Park J-W, Yip AC (2019) Photocatalysts for degradation of dyes in industrial effluents: Opportunities and challenges. Nano Res 12:955

[4] Balasurya S, Das A, Alyousef AA, Alqasim A, Almutairi N, Khan SS (2021) Facile synthesis of Bi2MoO6-Ag2MoO4 nanocomposite for the enhanced visible light photocatalytic removal of methylene blue and its antimicrobial application. J Mol Liquids 337:116350

[5] Mahanthappa M, Kottam N, Yellappa S (2019) Enhanced photocatalytic degradation of methylene blue dye using CuSCdS nanocomposite under visible light irradiation. Appl Surf Sci 475:828

[6] Ma M, Yang Y, Chen Y et al (2021) Photocatalytic degradation of MB dye by the magnetically separable 3D flower-like $Fe_3O_4/SiO_2/MnO_2/BiOBr$-Bi photocatalyst. J Alloys Compd. 861:158256

[7] Elgorban AM, Al Kheraif AA, Syed A (2021) Construction of Ag2WO4 decorated CoWO4 nano-heterojunction with recombination delay for enhanced visible light photocatalytic performance and its antibacterial applications. Colloids Surf A Physicochem Eng Asp 629:127416

[8] Kaliraj L, Ahn JC, Rupa EJ, Abid S, Lu J, Yang DC (2019) Synthesis of panos extract mediated ZnO nano-flowers as photocatalyst for industrial dye degradation by UV illumination. J Photochem Photobiol B Biol 199:111588

[9] Kurniawan TA, Mengting Z, Fu D et al (2020) Functionalizing TiO_2 with graphene oxide for enhancing photocatalytic degradation of methylene blue (MB) in contaminated wastewater. J Environ Manage 270:110871

[10] Chauhan PS, Kant R, Rai A, Gupta A, Bhattacharya S (2019) Facile synthesis of ZnO/GO nanoflowers over Si substrate for improved photocatalytic decolorization of MB dye and industrial wastewater under solar irradiation. Mater Sci Semicond Process 89:6

[11] Alhadhrami A, Almalki A, Adam AMA, Refat MS (2018) Preparation of semiconductor zinc oxide nanoparticles as a photocatalyst to get rid of organic dyes existing factories in

exchange for reuse in suitable purpose. Int J Electrochem Sci 13:6503

[12] Isac L, Cazan C, Enesca A, Andronic L (2019) Copper sulfide based heterojunctions as photocatalysts for dyes photodegradation. Front Chem 7:694

[13] Singh G, Panday S, Rawat M, Kukkar D, Basu S (2017) Nano Res. Trans Tech Publ

[14] Shaban M, Ahmed AM, Shehata N, Betiha MA, Rabie AM (2019) Ni-doped and Ni/Cr co-doped TiO_2 nanotubes for enhancement of photocatalytic degradation of methylene blue. J Colloid Interface Sci 555:31

[15] Zhang R, Ma Y, Lan W et al (2021) Enhanced photocatalytic degradation of organic dyes by ultrasonic-assisted electrospray TiO_2/graphene oxide on polyacrylonitrile/β-cyclodextrin nanofibrous membranes. Ultrason Sonochem 70:105343

[16] Zhu Q, Liu N, Zhang N et al (2018) Efficient photocatalytic removal of RhB, MO and MB dyes by optimized Ni/NiO/TiO_2 composite thin films under solar light irradiation. Chem Eng J 6:2724

[17] Dassanayake RS, Rajakaruna E, Abidi N (2018) Preparation of aerochitin-TiO_2 composite for efficient photocatalytic degradation of methylene blue. J Appl Polym Sci 135:45908

[18] Yan M, Wu Y, Liu X (2021) Photocatalytic nanocomposite membranes for high-efficiency degradation of tetracycline under visible light: An imitated core-shell Au-TiO_2-based design. J Alloys Compd 855:157548

[19] Zhang Y, Hu H, Chang M et al (2017) Non-uniform doping outperforms uniform doping for enhancing the photocatalytic efficiency of Au-doped TiO_2 nanotubes in organic dye degradation. Ceram Int 43:9053

[20] Ouyang H, Huang H, Wang H, Zheng X (2020) The morphology evolution of nitrogen-doped carbon quantum dots/hollow TiO_2 composites and their applications in photocatalysis. J Mater Sci 55:976

[21] Fatimah I, Nurillahi R, Sahroni I, Muraza O (2019) TiO_2-pillared saponite and photosensitization using a ruthenium complex for photocatalytic enhancement of the photodegradation of bromophenol blue. Appl Clay Sci 183:105302

[22] Du P, Song L, Xiong J, Cao H (2013) Photocatalytic degradation of Rhodamine B using electrospun TiO_2 and ZnO nanofibers: a comparative study. J Mater Sci 48:8386

[23] Jaleel UJR, Devi KS, Madhushree R, Pinheiro D (2021) Statistical and experimental studies of MoS_2/gC_3N_4/TiO_2: a ternary Z-scheme hybrid composite. J Mater Sci 56:6922

[24] Geetha N, Sivaranjani S, Ayeshamariam A et al (2018) High performance photo-catalyst based on nanosized ZnO–TiO_2 nanoplatelets for removal of RhB under visible light irradiation. J Microsc 13:12

[25] Ibrahim YO, Hezam A, Qahtan T, Al-Aswad A, Gondal M, Drmosh Q (2020) Laser-assisted synthesis of Z-scheme TiO_2/rGO/g-C_3N_4 nanocomposites for highly enhanced photocatalytic hydrogen evolution. Appl Surf Sci 534:147578

[26] Janani B, Syed A, HA AL-Shwaiman, MM Alkhulaifi, AM Elgorban, SS Khan, (2021) Performance analysis of novel $Bi_6Cr_2O_{15}$ coupled Co_3O_4 nano-heterostructure constructed by ultrasonic assisted method: Visible-light driven photocatalyst and antibacterial agent. Colloids Surf A Physicochem Eng Asp 622:126671

[27] Tran VA, Phung TK, Vo TK et al (2021) Solar-light-driven photocatalytic degradation of methyl orange dye over Co_3O_4-ZnO nanoparticles. Mater Lett 284:128902

[28] Saeed M, Muneer M, Mumtaz N, Siddique M, Akram N, Hamayun M (2018) Ag-Co_3O_4: Synthesis, characterization and evaluation of its photo-catalytic activity towards degradation of rhodamine B dye in aqueous medium. Chin J Chem Eng 26:1264

[29] Chinnathambi A, Nasif O, Alharbi SA, Khan SS (2021) Enhanced optoelectronic properties of multifunctional $MnFe_2O_4$ nanorods decorated Co_3O_4 nanoheterostructure: Photocatalytic activity and antibacterial behavior. Mater Sci Semicond Process. 134:105992

[30] Wang Y, Zhu C, Zuo G et al (2020) 0D/2D Co_3O_4/TiO_2 Z-Scheme heterojunction for boosted photocatalytic degradation and mechanism investigation. Appl Catal B 278:119298

[31] Janani B, Al-Kheraif AA, Thomas AM et al (2021) Construction of nano-heterojunction $AgFeO_2$–ZnO for boosted photocatalytic performance and its antibacterial applications. Mater Sci Semicond Process 133:105924

[32] Chen X, Liu L, Huang F (2015) Black titanium dioxide (TiO_2) nanomaterials. Chem Soc Rev 44:1861

[33] Mousavi M, Ghasemi JB (2021) Novel visible-light-responsive Black-TiO_2/$CoTiO_3$ Z-scheme heterojunction photocatalyst with efficient photocatalytic performance for the degradation of different organic dyes and tetracycline. J Taiwan Inst Chem Eng 121:168–183

[34.] Ran H, Fan J, Zhang X, Mao J, Shao G (2018) Enhanced performances of dye-sensitized solar cells based on Au-TiO_2 and Ag-TiO_2 plasmonic hybrid nanocomposites. Appl Surf Sci 430:415

[35] Ling L, Feng Y, Li H et al (2019) Microwave induced surface enhanced pollutant adsorption and photocatalytic degradation on Ag/TiO_2. Appl Surf Sci 483:772

[36] Li S, Wei X, Zhu S, Zhou Q, Gui Y (2021) Low temperature carbon monoxide gas sensor based on Co_3O_4@TiO_2 nanocomposites: theoretical and experimental analysis. J Alloys Compd 882:160710

[37] Jiang K, Liu B, Luo M et al (2019) Single platinum atoms embedded in nanoporous cobalt selenide as electrocatalyst for accelerating hydrogen evolution reaction. Nat Commun 10:1

[38] Lu Y, Yin W-J, Peng K-L et al (2018) Self-hydrogenated shell promoting photocatalytic H_2 evolution on anatase TiO_2. Nat Commun 9:1

[39] Shen L, Xing Z, Zou J et al (2017) Black TiO_2 nanobelts/ gC_3N_4 nanosheets laminated heterojunctions with efficient visible-light-driven photocatalytic performance. Sci Rep 7:41978

[40] Xing M, Zhang J, Chen F, Tian BJCC (2011) An economic method to prepare vacuum activated photocatalysts with high photo-activities and photosensitivities. Environ Sci Technol 47:4947

[41] Dong J, Han J, Liu Y et al (2014) Defective black TiO_2 synthesized via anodization for visible-light photocatalysis. ACS Appl Mater Interfaces 6:1385

[42] Rupa AV, Divakar D, Sivakumar T (2009) Titania and Noble Metals Deposited Titania Catalysts in the Photodegradation of Tartazine. Catal Lett 132:259. https://doi.org/10.1007/s10562-009-0108-7

[43] Liu M, Li H, Wang W (2016) Defective TiO_2 with oxygen vacancy and nanocluster modification for efficient visible light environment remediation. Catal Today 264:236

[44] Ali G, Zaidi SJA, Basit MA, Park TJ (2021) Synergetic performance of systematically designed g-C3N4/rGO/SnO2 nanocomposite for photodegradation of Rhodamine-B dye. Appl Surface Sci 570:151140

[45] Wang Q, Zhang L, Guo Y et al (2020) Multifunctional 2D porous g-C3N4 nanosheets hybridized with 3D hierarchical TiO2 microflowers for selective dye adsorption, antibiotic degradation and CO2 reduction. Chem Eng J 396:125347

[46] Ling F, Jing H, Chen Y et al (2018) Metastable phase control of two-dimensional transition metal dichalcogenides on metal substrates. J Mater Chem C 6:12245

[47] Sobana N, Muruganadham M, Swaminathan M (2006) Nano-Ag particles doped TiO_2 for efficient photodegradation of direct azo dyes. J Mol Catal 258:124

[48] Demirci S, Dikici T, Yurddaskal M, Gultekin S, Toparli M, Celik E (2016) Synthesis and characterization of Ag doped TiO_2 heterojunction films and their photocatalytic performances. Appl Surf Sci 390:591

[49] Gao F, Yang Y, Wang T (2015) Preparation of porous TiO_2/ Ag heterostructure films with enhanced photocatalytic activity. Chem Eng J 270:418

[50] Shi Y, Yang D, Li Y, Qu J, Yu Z-ZJASS (2017) Fabrication of PAN@ TiO_2/Ag nanofibrous membrane with high visible light response and satisfactory recyclability for dye photocatalytic degradation. Appl Surf Sci 426:622

[51] Billo T, Fu FY, Raghunath P et al (2018) Ni-Nanocluster Modified Black TiO_2 with Dual Active Sites for Selective Photocatalytic CO_2 Reduction. Small 14:1702928

[52] Leong KH, Gan BL, Ibrahim S, Saravanan PJASS (2014) Synthesis of surface plasmon resonance (SPR) triggered Ag/ TiO_2 photocatalyst for degradation of endocrine disturbing compounds. Appl Surf 319:128

[53] Kokilavani S, Syed A, Thomas AM et al (2021) Integrating Ag2WO4 on VS4 nanoplates with synergy of plasmonic photocatalysis and boosted visible-light harvesting and its antibacterial applications. J Alloys Compounds 865:158810

[54] Low J, Qiu S, Xu D, Jiang C, Cheng BJASS (2018) Direct evidence and enhancement of surface plasmon resonance effect on Ag-loaded TiO_2 nanotube arrays for photocatalytic CO_2 reduction. Appl Surf 434:423

[55] Coto M, Divitini G, Dey A et al (2017) Tuning the properties of a black TiO_2-Ag visible light photocatalyst produced by a rapid one-pot chemical reduction. Mater Today 4:142

[56] Huang B, Yang W, Wen Y, Shan B, RJAam Chen, interfaces, (2015) Co_3O_4-modified TiO_2 nanotube arrays via atomic layer deposition for improved visible-light photoelectrochemical performance. ACS Appl Mater Interfaces 7:422